Effect of anisotropy on Fatigue properties of AA2198 Al-Li plates joined by Friction Stir Welding

P. Cavaliere, A. De Santis
Dept. of Innovation Engineering, University of Salento, Lecce, Italy

ABSTRACT

Al-Li alloys are characterized by a strong anisotropy in mechanical and microstructural properties with respect to the rolling direction. In the present paper sheets, 4 mm thick, of AA2198 Al-Li alloy were joined via Friction Stir Welding (FSW) by employing a rotating speed of 1000 RPM and a welding speed of 80 mm/min, in parallel and orthogonal direction with respect to the rolling one. The joint mechanical properties were evaluated by means of tensile tests at room temperature. In addition, fatigue tests were performed by using a resonant electro-mechanical testing machine under constant amplitude control up to 250 Hz sinusoidal loading. The fatigue tests were conducted in axial control mode with $R=\sigma_{min}/\sigma_{max}=0.33$, for all the welding and rotating speeds conditions. The damage behavior was studied by applying thermoelastic stress analysis (TSA) to the crack formation and propagation of friction stir welded sheets under cyclic fatigue tests. The fatigue crack propagation experiments were performed on single edge notched specimens. Fatigue tests were carried out up to failure in tension-tension with load ratio R=0.33. The TSA measurement system allowed crack evolution to be observed in real-time during fatigue cycles and stress fields to be derived on the specimens from the temperature variation. The thermoelastic data were used to measure the principal stresses and principal strains on the specimens surface and the crack growth rate during tests. All the results were validated by employing finite element analysis performed with ABAQUS software. SEM observations of the fractured surfaces were done to characterize the weld performances.

RIASSUNTO

Le leghe Al-Li mostrano una forte anisotropia nelle proprietà meccaniche e microstrutturali in funzione della direzione di laminazione. Nel lavoro sono presentati i risultati relativi allo studio di saldature ottenute mediante "fiction stir welding" (FSW) di laminati della lega AA2198 spessi 4 mm; le saldature sono state effettuate con una velocità di rotazione dell'utensile di 1000 RPM e velocità di avanzamento di 80 mm/min. Sono stati studiati i giunti di saldatura eseguiti nelle direzioni parallela e ortogonale rispetto a quella di laminazione della lamiera. Le proprietà meccaniche a temperatura ambiente sono state ricavate mediante prove di trazione e di fatica ad elevata frequenza (250 Hz), con un valore di $R=\sigma_{min}/\sigma_{max}$ pari a 0.33. Le prove di fatica sono state effettuate su provini pre-criccati; la nucleazione e la propagazione del danneggiamento sono state rilevate mediante l'analisi termo-elastica e mediante l'utilizzo di una camera CCD ad alta frequenza. I dati termoelastici sono stati utilizzati per ricavare sia i valori di tensione e deformazione principali durante la prova che la velocità di nucleazione e propagazione delle cricche di fatica. Tutti i risultati sono stati validati mediante l'analisi agli elementi finiti utilizzando il codice commerciale ABAQUS. Le superfici di frattura dei provini testati sono state studiate mediante microscopia elettronica in scansione.

KEYWORDS

Friction Stir Welding; Al-Li; Fatigue; Fatigue crack behavior; Thermoelastic stress analysis.

INTRODUCTION

The Friction Stir Welding technology is being targeted by modern aerospace industry for high performance structural applications [1]. If compared to traditional welding techniques, FSW strongly reduces the presence of distortions and residual stresses [2-4]. Based on friction heating at the facing surfaces of two sheets to be joined, in the FSW process a special tool with a properly designed rotating probe travels down the length of contacting metal plates, producing an highly plastically deformed zone through the associated stirring action. The localized thermo-mechanical affected zone is produced by friction between the tool shoulder and the plate top surface, as well as plastic deformation of the material in contact with the tool [5]. The probe is typically slightly shorter than the thickness of the work-piece and its diameter is typically slight larger than the thickness of the work piece [6]. The microstructure evolution and the resulting mechanical properties depend strongly on the variation of the processing parameters leading to a wide range of possible performances [7]. The FSW process is a solid state process and therefore solidification structure is absent in the weld and the problem related to the presence of brittle inter-dendritic and eutectic phases is eliminated [7]. Some aluminium alloys can be resistance welded with an extensive surface preparation due to oxide formation. On the other hand, FSW can be used to join most Al alloys as the surface oxide is not a deterrent for the process and therefore no particular cleaning operation is needed prior to welding. In FSW the work-piece does not reach the melting point and the mechanical properties of the welded zone (especially when attention is focused on heat-treatable light alloys) are much higher compared to those provided by traditional techniques. In fact, the undesirable low mechanical properties microstructure resulting from melting and re-solidification is absent in FSW welds leading to improved mechanical properties, such as ductility and strength in some alloys [8-12]. In this way, the welds are characterized by low distortion, lower residual stresses and absence of micro defects and then of retained products dimensional stability.

Fatigue is the principal cause of failure for welded joints in mechanical components; the application of FSW technology is in particular dependence on mechanical performances, which are strongly affected by the processing parameters, as James et al. [13] showed the different fatigue behaviour of two Al-Mg alloys as a function of welding speed. In addition, Sandtrom et al. [14] showed the variation of fatigue life of AA6082 joints with the welding speed, comparing the results with conventional fusion welding techniques. Al-Mg and Al-Mg-Si alloys plates of different thickness, joined with different welding speeds, have been studied also by Dickerson et al. [15]. Recently some papers were published regarding the microstructural and mechanical properties of friction stir welded Al-Li alloys. In particular Hao et al. presented interesting results of tensile and bending properties as a function of processing parameters in the AA1420 [16]. The paper aims at shading light on the anisotropy evolution of the plates undergone FSW.

EXPERIMENTAL PROCEDURE

MATERIALS AND METHODS

The material under investigation was the AA2198-T851, produced by ALCAN in form of rolled sheets, 5 mm thick, with the following composition (wt%): Si 0.03, Fe 0.04, Cu 3.3, Mn 0.01, Mg 0.32, Cr 0.01, Ni 0.01, Zn 0.02, Ti 0.03, Zr 0.11, Pb 0.01, Li 1.0, Al bal. Rectangular plates 200 mm x 80 mm were welded in perpendicular and parallel direction with respect to the rolling one. The rotating velocity (in clockwise direction) of the cylindrical threaded tool was 1000 RPM while the advancing speed was 80 mm/min, the tilt angle was set equal to 2°. The flat tool geometry dimensions are reported in Table I.

Table 1. Tool geometry

Tool parts	Dimensions (mm)
Pin length	4,64
Pin diameter	5,67
Shoulder diameter	9,5

Some sheets were instrumented with K-type thermocouples embedded in different position, in order to monitor the temperature profiles as a function of the distance from the weld line. The evaluation of the joint mechanical properties was performed by means of tensile tests carried out at room temperature. Specimens 12 mm wide, 80 mm long and with 25mm gauge length, were tested in tension by using a MTS 810 machine with initial strain rate of $10^{-3}s^{-1}$. The residual stresses were calculated in longitudinal direction, respect to the loading one, by employing the sin2Ψ method [17].

Endurance fatigue tests were performed by a resonant electro-mechanical testing machine, TESTRONICTM 50±25 kN, under constant loading control up to 250 Hz sine wave loading in both low and high regimes. The cyclic fatigue tests were conducted under axial total stress amplitude control mode under fully reversed, push-pull, tension loading ($R=\sigma_{min}/\sigma_{max}=0.33$). The fatigue specimen gauge dimensions measured 12.5 mm in width, 50 mm in length. All the mechanical tests were performed up to failure. The fatigue crack propagation experiments were performed with the same machine and by employing single edge (1 mm) notched specimens obtained on the advancing side. The FSW, in fact, does not produce a symmetric deformation respect to the centre line of the advancing tool [18]. Due to such inhomogeneities, when a clock wise direction rotation is employed the less resistant zone results the one on the advancing side of the tool. From previous studies on AA6082 [19] the fractured zone for tensile and fatigue specimens resulted the one on the advancing side of the tool. In such experiments a clock wise direction rotation was employed in a wide range of processing speeds. For all tested materials, R=0.33 was used.

Specimens for the microstructural analyses were prepared by standard metallographic techniques and etched with Keller's reagent to reveal the grain structure.

A FEGSEM (JEOL-JSM 6500 F) was used to study the fracture surfaces of the material after tensile and fatigue tests.

PRINCIPLES OF TSA

Few papers exist on the evaluation of fatigue behavior of materials using thermographic infrared techniques [20-24]. These techniques are contactless and able to investigate areas rather than just single surface points. No special sample treatment is necessary and the measurement technique therefore does not require a long preparation time. Analysis of the stress fields around a crack tip is performed starting from 2D images which show the temperature distribution over the sample surface. In recent years IR cameras which allow those measurement have drastically improved both the spatial resolution and temperature recording speed. Crack propagation has been more and more studied in the last two decades using the SPATE (stress pattern analysis by thermal emission) system [25], which has allowed the determination of crack growth rate based on the evaluation of the thermoelastic effect. Special IR cameras called "differential cameras" have been developed to analyze the different temperature component and therefore the thermoelastic effect rather than the overall temperature variation (due also to the inelastic and the heat conduction effects), as in classical thermography measurements. In particular, the signal from the infrared camera is sampled in correspondence of the positive and negative peaks of the reference signal. In this way a signal proportional to the thermoelastic effect due to the cyclic loading is obtained. Studies on fatigue crack initiation and propagation are therefore made possible over areas of the sample surface with lower uncertainty, high spatial and time resolution. Relevant advantages related to the use of these technique have also allowed the determination of the stress intensity factor from thermoelastic data. The DeltaTherm system makes it possible to actually perform real-time investigation of the crack propagation based on faster data collection [26]. This opens up the possibility of identifying in real-time, i.e. while the test is actually being carried out, the presence of crack initiation and propagation [27, 28]. Thermoelasticity is based on the fact that under adiabatic and reversible conditions, a cyclically loaded structure undergoes temperature variations which are directly proportional to the sum of the principal stresses. To achieve adiabatic conditions in the laboratory practice, the test sample is cyclically loaded at frequencies higher than 10 to 40 Hz. Measurement by the thermoelastic technique allows therefore the determination of superficial stress through the evaluation of superficial temperature variations related to a cyclic load [29, 30]. The measurement system used in this work is composed by: a DeltaTherm 1560 IR camera in which the sensitive element is a CCD IR focal plane array; a Lock-in system necessary to synchronize the acquisition with the external load; a thermal image post-processing software. The maximum resolution that can be obtained in terms of averaged temperature difference is in the order of some mK [31-34]. Suitable optics concentrate the stress analysis on 256x320 points on an area of 3x4 mm in order to analyze very small details and locations where high stress gradient takes place, actually with a spatial resolution up to 22 μm. Assuming adiabatic conditions, it becomes possible to establish a linear relationship between the mechanical energy and the thermal energy. For a linear elastic, isotropic, homogeneous material a linear relationship between the sum of the two principal stresses Δs with the amplitude of the output signal V from each pixel of the thermographic array (proportional to temperature fluctuations) may be obtained [34, 35]:

$$Ds = \frac{D \times R \times \rho \times C_p}{\alpha \times T \times \zeta} \times V \qquad (1)$$

where D is a calibration factor depending on the difference between the measured superficial stress and a reference signal controlling the frequency variation, R is a correction factor which compensates for temperature-dependent changes in radiation intensity and wavelength (the instrument is very sensitive and compensates the stress measurement values variation as a function of the temperature fluctuations on the specimen surface), ρ is the material density, Cp is the specific heat at constant pressure, α is the coefficient of thermal expansion, T is the absolute temperature, ζ is the surface emissivity. The resolutions that can be achieved in terms of stress depends on the material characteristics: they are typically 1 MPa for steel and 0.4 MPa for aluminium [32-35].
The scale factor between the sum of the principal strains and the amplitude of the output signal from each pixel of the termographic array can be calculated by the following equation:

$$K = \frac{E(\varepsilon_x + \varepsilon_y)}{V(1 - \nu)} \qquad (2)$$

where E is the Young modulus of the material, ν is the Poisson ratio, $(\varepsilon_x+\varepsilon_y)$ is the sum of the principal strains and V is the root mean square of the signal measured by each infrared sensor of the thermographic array [33].
For Mode I the characteristic stress intensity factor can be calculated by [36]:

$$J = \left(\frac{EG}{1-(\alpha\nu)}\right)^{\frac{1}{2}} \qquad (3)$$

ν is the Poisson ratio and G tangential modulus. The evaluation of the characteristic fracture parameters for the studied joints was performed by employing finite element simulations by ABAQUS software.
The mesh used for the simulations was built up by using 4-nodes elements, different numbers of elements were used to model the small scale yielding problem for the different studied configurations. The crack propagation zone simulation was performed by employing 1558 elements. The specimen geometry were 25 mm height, 10.5 mm wide and 1 mm notch.
The materials behaviour was considered to be governed by the rate-independent theory of plasticity with isotropic hardening. The loads were applied in an incremental way, and the solution to the non linear boundary value problem at each increment was obtained by a fully implicit update using the Newton-Rapson method [37].

RESULTS AND DISCUSSION

FRICTION STIR WELDING STUDIES

FSW has become a very effective tool in solving the joining problems of profiled sheets with material continuity, without using different joining methods; particularly in case of aerospace industry, where high ductility and tensile strength are required. In the present work, different FSW butt welds of AA2198 sheets were successfully obtained by varying the welding orientation respect to the rolling one; no superficial or macroscopic defects, Figure 1, were observed on the surfaces and the welded joints where mechanically and microstructurally characterized.

THERMO-MECHANICAL JOINTS BEHAVIOR

The thermal behavior of the different material zones during FSW was monitored by measuring the temperature with K-type thermocouples of 2 mm in diameter. Different thermocouples configurations were used in order to map the thermal history of the material as shown in Figure 2. The thermal history for the two welding configurations leds to different profiles in the microhardness measurements. In Figure 3 the microhardness profiles for the L and T welds and the mechanical properties are plotted in the same graphs with the provisional thermal profiles obtained by the polynomial fit calculated from the measured temperatures. For both the cases, the maximum measured temperature (at a distance of 10 mm from the centerline) was close to 250°C and then decreases by increasing the distance; for both the welding configurations, the temperature behavior is very similar. In all the measurements, the temperatures in the retreating sides resulted lower, respect to the advancing one, by increasing the distance from the welds centerline. For the L welding configuration, the absolute temperatures resulted higher (in the same zone) respect to the T configuration.

In the case of L configuration it seems that the material is less effective in dissipating the thermal energy developed by the tool movement, in fact, for both the configurations the highest temperature is very similar (close to 320 °C in the center of the nugget zone) but the profile describes that the temperature decreases much more faster in the T configuration with respect to the L one. Such behavior is confirmed by the microhardness values; for example at 5 mm from the centerline on the advancing side it can be noted the classical overageing behavior of FSW material with a strong softening due to the coupled effect of temperature and forging-extrusion of the material; the hardness value is very close (90-95 HV) for both the welds. By increasing the distance from the centerline in the case of T configuration the temperature starts to decrease faster respect to the L one and in fact in this case the softening zone appears broader respect to the T weld.

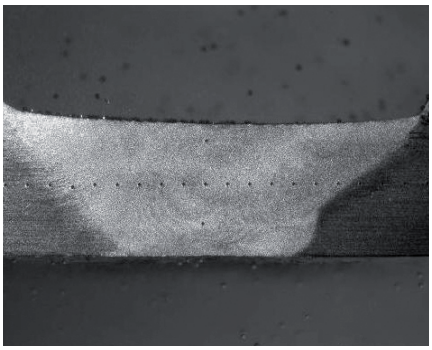

Fig. 1: Optical micrograph of a joint cross section.

MECHANICAL PROPERTIES

The base metal tensile properties of AA2198-T851 sheets are described in Table II for both the T and L directions. The mechanical strength of the base material results much more higher in the L direction respect to the T one and accompanied with a reduction in ductility and an increase in the necking value, demonstrating the strong anisotropy of such kind of Al-Li alloys with respect to the rolling direction. Many different specimens in the two friction stir

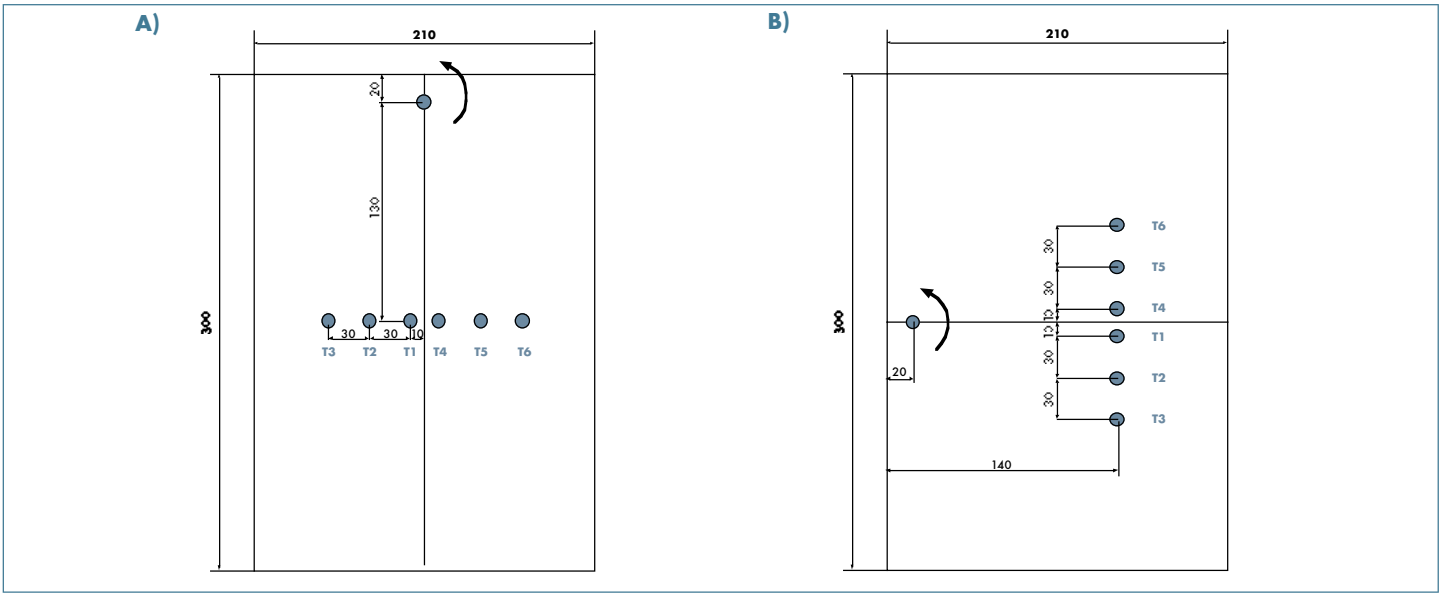

Fig. 2: Thermocouple arrangement for the temperatures profile measurement during the joining process: a) Transversal b) Longitutinal direction.

welded configurations were tested in fatigue to study the behavior of the material after joining. The fatigue properties of the FS Welded joints can be observed in S-N curves for the toughest studied joints, as shown in Figure 4. The fatigue specimens have been cut from the welded plates in a number of 25 for each condition and polished, according to standard procedures and avoiding superficial defects. The bead material in all the welding configurations shows similar fatigue behavior in the low cycle regime, since extremely narrow data differences are produced in terms of stresses especially in the intermediate region; in the high cycle regime, the Wöhler curves did not show clear differences. It can be observed decreasing stress amplitude limits as function of life endurance up to the fatigue limit (~$4x10^6$ cycles to failure) and such a value is very similar for both the configurations at a value of the cyclic stress amplitude of 140 MPa. On the contrary, the base materials show a strong difference in the fatigue life and in particular in the fatigue limit (220 MPa for the L direction, 180 MPa for the T direction in terms of stress amplitude).

In different configuration and with the same used welding parameters it was reached a good combination between the material plasticization during tool rotation and the mixing affect produced by the advancing movement leading to the disappearance of the effects due to the rolling process. The tool advancing action (inclined at a certain angle) is extremely similar to an extrusion process which requires optimal temperature conditions for the better quality of the material in terms of microstructure; consequently, since the resultant fatigue behavior for butt welded joints is directly related to the microstructure, provided that porosities occurrence is avoided and micro-cracks formation is absent, and considering that stress concentrators are missing, the studied FS Welded joints offer the best fatigue performances only when optimal microstructure configurations are reached. With a revolutionary pitch in the range of 0.07 – 0.1 [19], the process is in the optimal temperature and strain rates conditions to produce good microstructure quality without defects for butt joints and therefore sound welds are achieved. The longitudinal residual stresses were measured in the cross sections of the welds by X-ray diffraction using the sin2Ψ method [38]. Residual stress profiles of the two studied joints configuration is shown in Figure 5. It must be observed that the residual stresses can be relaxed for the cut of the mechanical testing specimens, for this reason the residual stresses showed in the present work are related to the measurements performed on the cut material. As a general behavior, the residual stresses have compressive character by approaching the weld line, changing to a tensile character in the weld zone from the heat affected one. It can be observed that the higher values of residual stresses are achieved in the advancing side of the tool, the profiles show a very similar

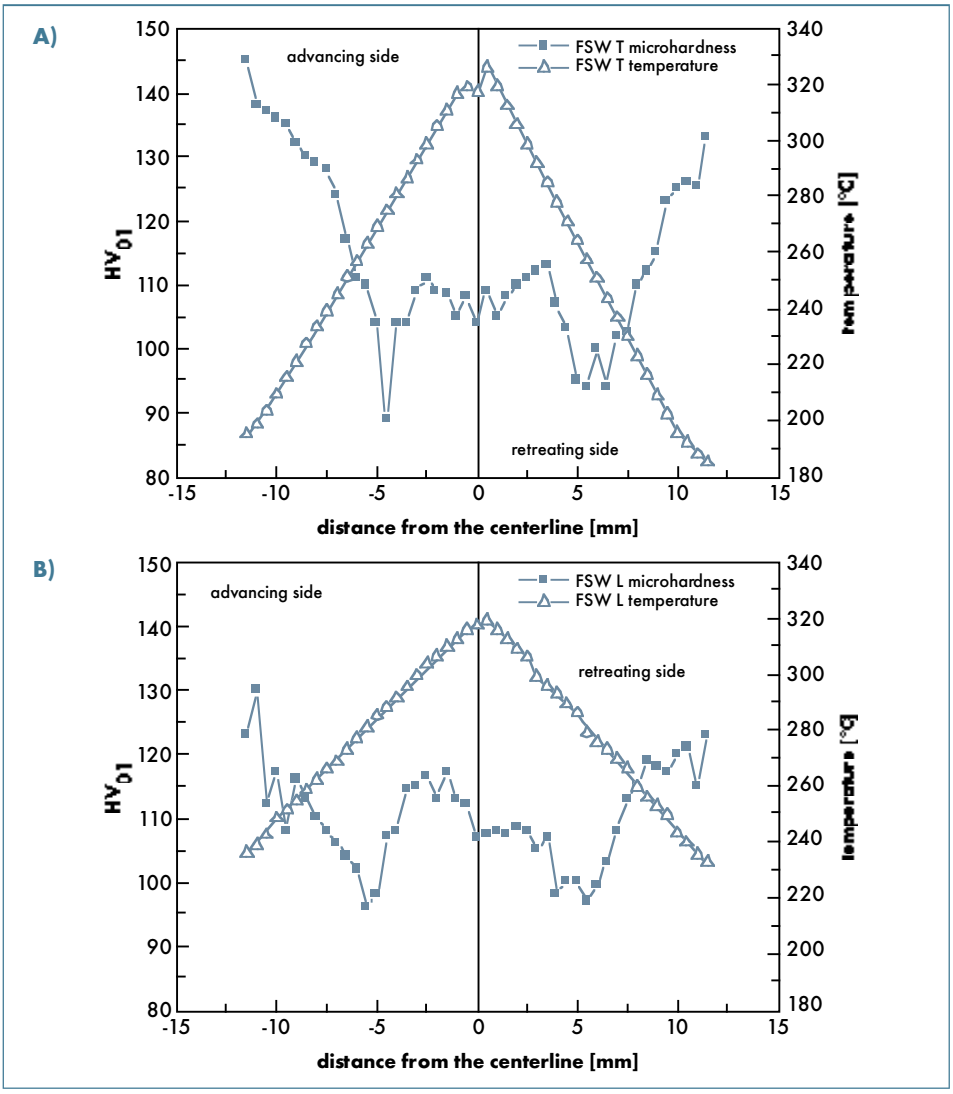

Fig. 3: Temperature profiles coupled with the microhardness values, in the T(a) and L(b) configurations, on both the advancing and the retreating sides of the tool.

Table II. Mechanical properties of the base metal in both directions

Alloys	σ_y (MPa)	UTS (MPa)	E (GPa)	ε	A (%)
AA2198-T	347	431	74.3	0.2	18.3
AA2198-L	436.3	490.7	76.7	0.16	13.7

behavior in both the configurations with higher values experienced in the case of T joints. The residual stresses values differences depend on the asymmetry of the FSW process; it is demonstrated by several finite element calculations that the higher deformation across the weld line are achieved in the retreating side of the tool when a clockwise direction is employed for the rotation [39-42]. Such an higher deformation produces an increase in the temperature respect to the advancing side leading to a softening during the process. The small difference observed in the T and L configuration can be attributed to the fact that in the T configuration the main deformation acts perpendicularly to the main resistant direction of the sheets leading to an hardening respect to the L configuration.

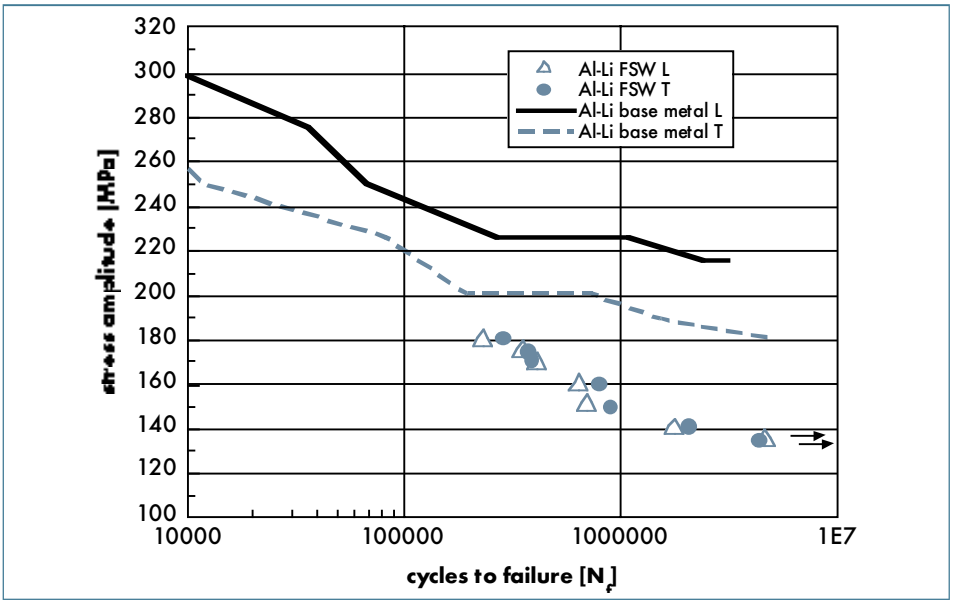

Fig. 4: Fatigue endurance curves of the friction stir welded AA2198 plates in both T and L directions, for comparison the data of the base materials are also plotted.

CRACK BEHAVIOR

All the fatigue crack tests were monitored via thermoelastic stress analysis. Thermoelastic stress analysis (TSA) provided the full field stress maps from the surface of the specimens subjected to cyclic loading. In order to achieve a higher resolution in the stress spatial distribution, the investigating area was restricted using suitable optics around the region where crack initiation was observed during preliminary tests. In all the test conditions, the crack initiation leading to the samples failure was observed in real-time from the thermal images. As already mentioned, when the material is loaded at high frequency in the elastic region, the thermoelastic data relative to the conduction are linearly proportional to the sum of principal stresses. Crack formation and propagation can be followed in real-time providing continuously the real stress fields around the crack tip, including closure effects.

All the stress maps were obtained using the scale factor K calculated following Eq. (2) together with the output signal V from the measurement system in each measurement point and considering the material as isotropic and homogeneous. Eq. (2) requires also adiabatic conditions to hold and it is therefore important to find a way to verify that these are fulfilled, examining carefully the thermal images around the area of crack initiation. In the surroundings of this zone, adiabatic conditions may fail to verify. There are two basic phenomena that lead to a lack of adiabatic conditions and hence a change in phase: heat generation due to plastic work and the presence of high stress gradients. Both are conditions occurring near the crack tip area. The effect of these phenomena on the thermoelastic images is a blurring around the crack tip area which makes it difficult to determine crack tip only from observation. The exact location of the crack tip is important when, for example, the stress intensity factor is inferred from thermoelastic measured data. The loss of adiabaticity can be identified from the phase maps and from the examination of the different phase profiles. When adiabatic conditions are achieved the phase is constant and equal to zero. Observing the phase profile, three different zones can be identified approaching the crack tip area (see also [27]): i) a region where the phase is constant and therefore adiabatic conditions are achieved; ii) a

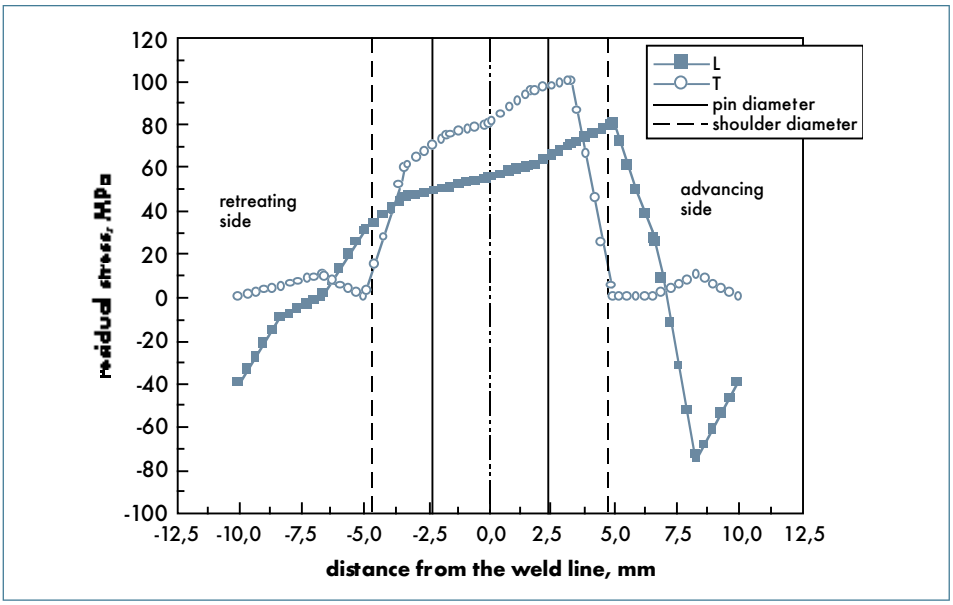

Fig. 5: Residual stress profiles for the FSW joints in both the studied configurations.

region where the phase starts assuming positive values indicating a loss of adiabaticity due to plasticity and high stress gradients; iii) a region where the phase changes to negative until the crack tip is reached, due probably to reverse plasticity effects. From the crack tip onwards the phase sign changes continuously, this fact being attributed probably to contact between the crack faces and background reflections coming from inside the crack. In this way it is possible to calculate the position of the end of third region during the fatigue tests in all the loading conditions relating it to the number of cycles. This data is used to infer the crack length and rate, Figure 6.

The change in the shape of the curves related to the stress fields is therefore due to the lack of adiabatic conditions and then to the different heat generation and conduction due to the plastic deformation of the material in the crack zone subjected to various cyclic loadings.

The principal stresses distribution directly measured and normalized around the crack site for different number of loading cycles is shown in Figure 7. An increase of the stress values around the crack site was observed as increasing the number of cycles, as expected. The broadening of stress profiles around the crack by increasing the cyclic loading reveals that the stress concentration zone increases also with stress.

The results of ABAQUS simulations were used to calculate the theoretical KI values at different crack lengths. In Figure 8 it is shown the Von Mises stress distribution around the crack tip for the specimen

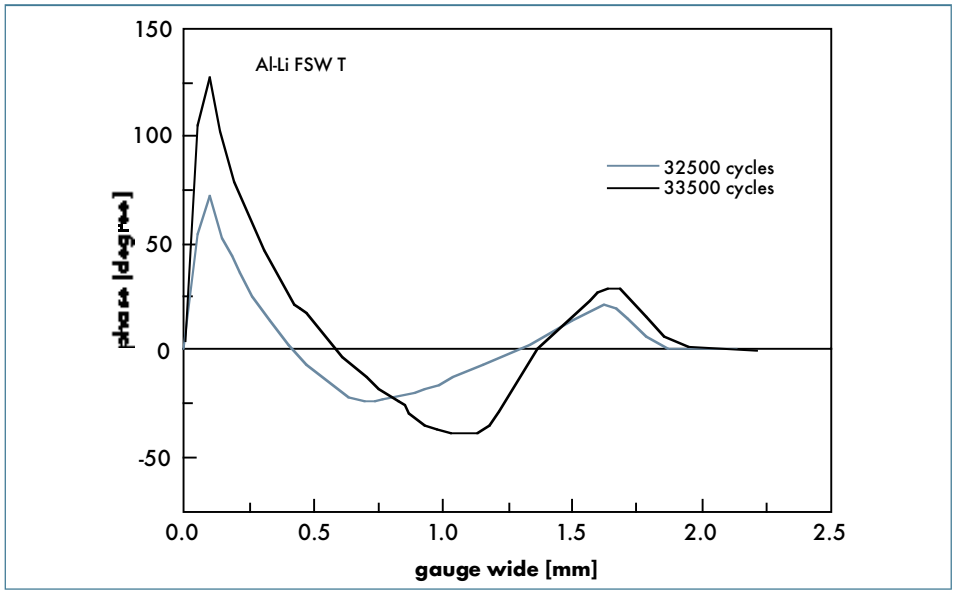

Fig. 6: Examples of different phase profiles, phase variation along lines at 32500 a) and 33500 b) cycles.

welded in the T configuration and the corresponding stress field map for a crack length of 2 mm. From the previous calculations, the stress intensity factor (SIF) values as a function of the crack lengths were obtained. In such calculations it was not considered the effect of residual stresses on the stress-field maps and consequently on the effective values of the stress intensity factors. To take into account such residual stresses effects it was calculated their contribution to the K_I as follow:

$$K_I = \int_0^a S_0(x)m(x,a)dx \qquad (4)$$

Where:

$$m(x,a) = \frac{\left[1 + m_1\left(1 - \frac{\chi}{a}\right) + m_2\left(1 - \frac{\chi}{a}\right)^2\right]}{\sqrt{2\pi(a - \chi)}}$$

$$m_1 = 0.6147 + 17.1844\left(\frac{a}{W}\right)^2 + 8.7822\left(\frac{a}{W}\right)^6$$

$$m_2 = 0.2505 + 3.2889\left(\frac{a}{W}\right)^2 + 70.0444\left(\frac{a}{W}\right)^6$$

S_0 is the residual stresses profile along the crack path, m(x,a) is a weight function, m_1 and m_2 are its coefficients.

The contribution due to the effect of crack aperture was estimated by the following equation:

$$K_{aperture} = C\sigma_{aperture}\sqrt{\pi a}$$

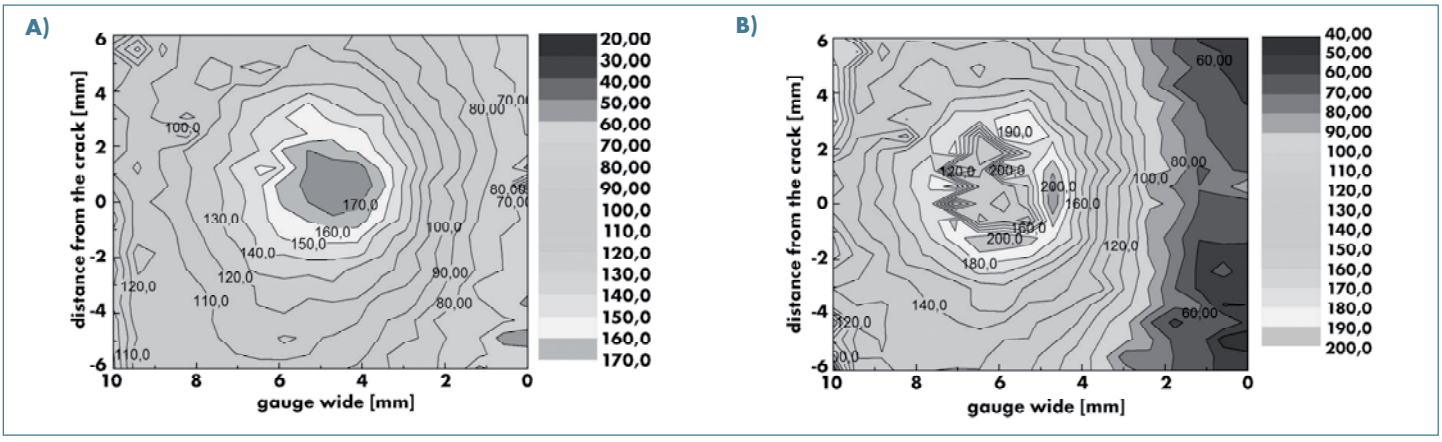

Fig. 7: Stress fields maps for the FSW joints welded in T configuration at 32500 a) and 33500 b) cycles.

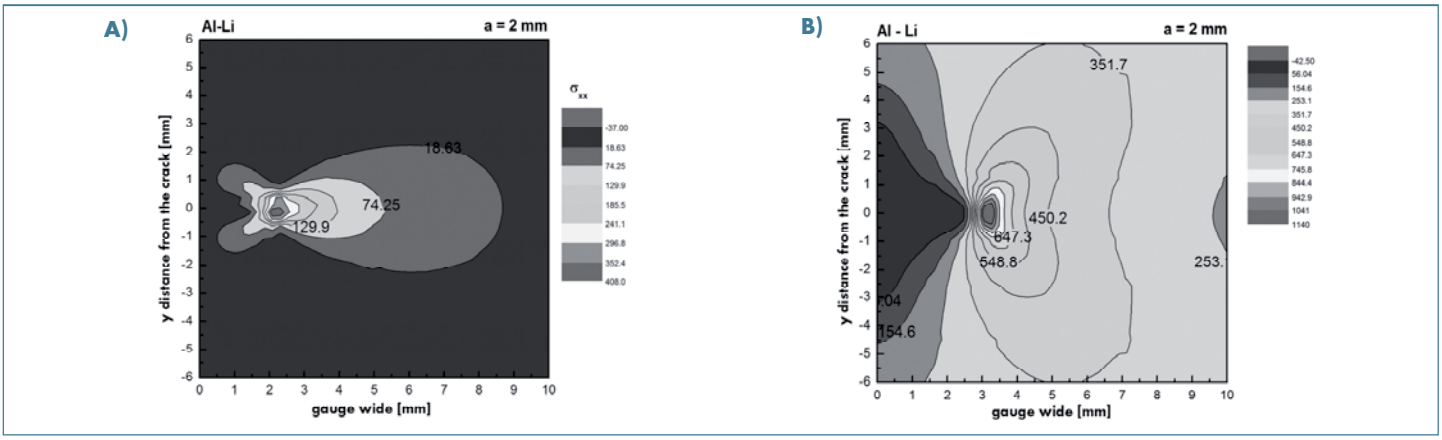

Fig. 8: Von Mises stress distribution around the crack tip for the specimen welded in the T configuration: a) σ_{xx}, b) σ_{yy}, and the corresponding stress field map for a crack length of 2 mm.

$$C = 1.12 - 0.231\left(\frac{a}{W}\right) + 10.55\left(\frac{a}{W}\right)^2 - 21.72\left(\frac{a}{W}\right)^3 + 30.39\left(\frac{a}{W}\right)^4 \quad (5)$$

In such a way it was possible to take into account all the phenomena affecting the deviation from the theoretical SIF value. The corrected KI behaviour as a function of the crack length compared with those belonging to the calculations performed with CCD camera observations and TSA is plotted in Figure 9. The crack initiation and growth behaviour, for both the studied configurations is shown in Figure 10. The fatigue crack growth rate results are shown in the curves processed at a load ratio of R = 0.33. Representative R-curves for the base material in longitudinal and transversal directions are shown in the same figure. The curves exhibit a rising behavior and substantial crack extension before the occurrence of plastic instability. The AA2198 showed an higher crack resistance in the longitudinal direction if compared with the transversal one.
Both the L and T welds show a similar behaviour in the crack initiation and growth leading to the conclusion that the FSW process eliminates the effect of rolling direction on the fatigue properties of the welds. As a general behaviour the experimental curves tend to underestimate the KI value at the same crack length, after few mm of crack propagation the TSA measurements are coincident with the theoretical model while the CCD camera calculations continue to underestimate the SIF.

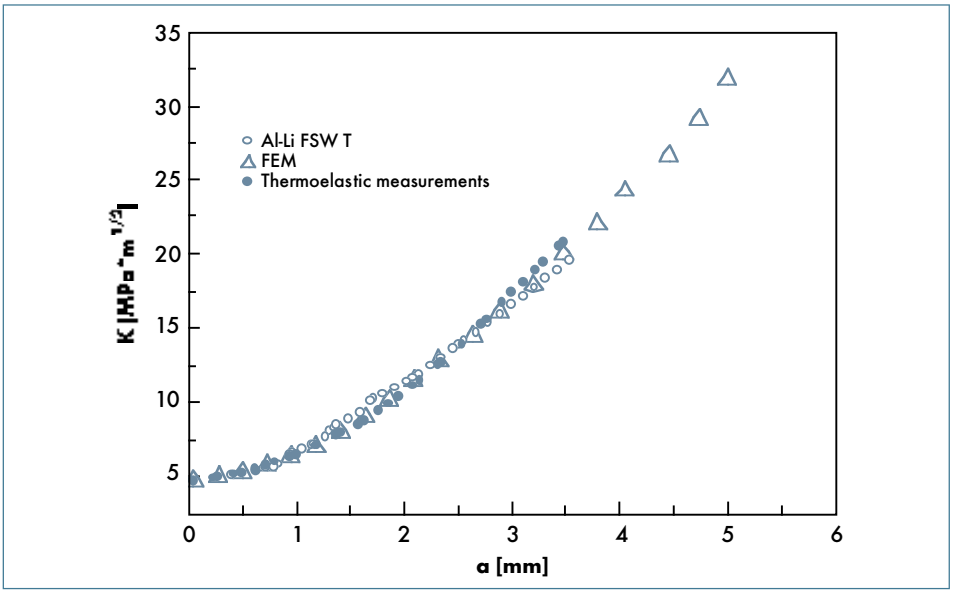

Fig. 9: K_I as a function of crack length for the specimen welded in T configuration calculated with FEM and measured with TSA and CCD observations.

FRACTOGRAPHY

The SEM observations of the fracture surfaces of the tensile specimens revealed a very similar behavior in both T and L welding configuration. The fracture surfaces appeared populated of fine dimples revealing a very ductile behavior of the material before failure, Figure 11. All the fatigue tested specimens was observed to fracture in the advancing side of the tool. The failure is related to the coalescence of many small voids and defects in the material. The presence of dimples on the surface revealed a local ductile behavior of the material prior to fracture. Such a behavior was observed on the whole fracture surface revealing the observations previously explained on the optimal deformation conditions (temperature and strain rate) necessary to obtain good quality material after deformation. This is the case of such conditions in which the optimal solution between material mixing and grain refinement is obtained. In all the specimens the main fracture mechanism results the cleavage accompanied with small specimen zones of local ductility aspect (dimples) and fatigue striations, Figure 12. This aspect has been attributed to the heating of the material during welding.

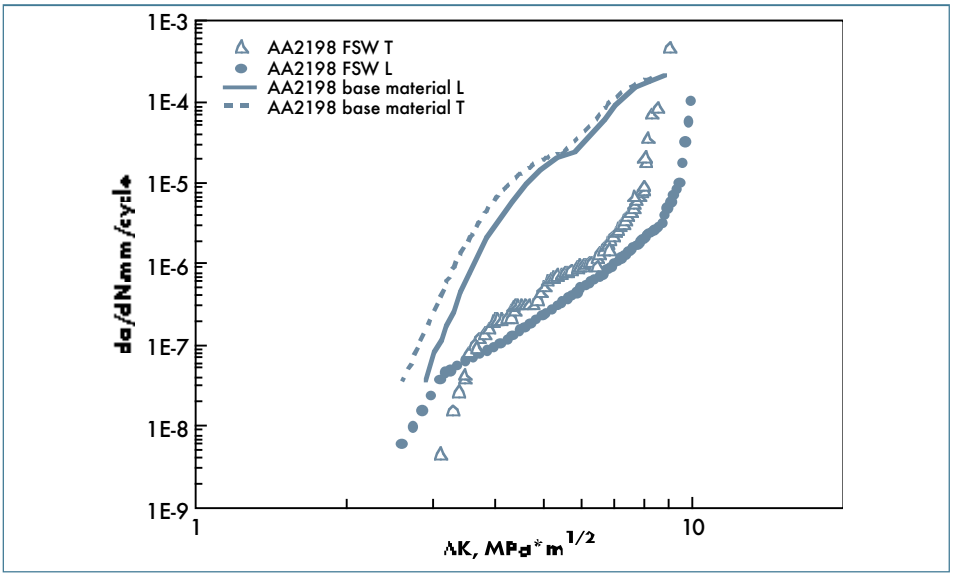

Fig. 10: Crack growth behaviour for the AA2198 plates friction stir welded in T and L configurations, for comparison the data of the base materials are plotted in the same graph.

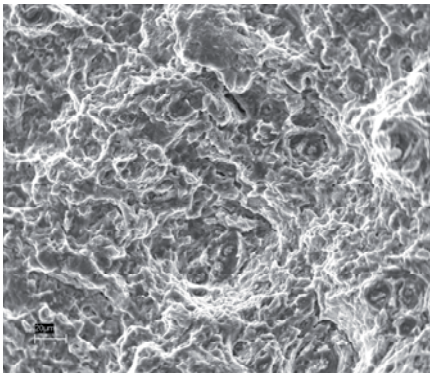

Fig. 11: Very fine dimples revealing a ductile behavior of the material before failure for T joints.

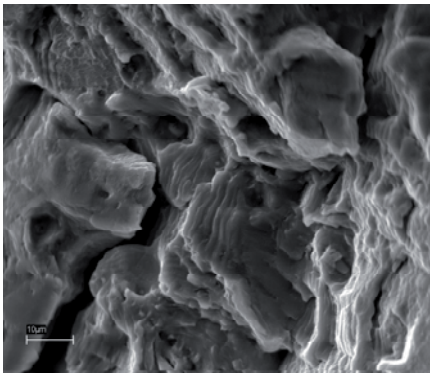

Fig. 12: Cleavage deformation accompanied with small specimen zones of local ductility aspect (dimples) and fatigue striations for T joints.

CONCLUSIONS

The effect of rolling direction respect to the welding one on the mechanical behavior of FSW Al-Li plates was studied and the results reported in the present paper. The thermal profiles of the material during welds was very similar for both the configurations with a temperature of 250°C at 10 mm from the centerline to 320°C in the center of the welds. The mechanical strength of the base material results much more higher in the L direction respect to the T one accompanied with a reduction in ductility and an increase in the necking value, demonstrating the strong anisotropy of such kind of Al-Li alloys with respect to the rolling direction. In the high cycle fatigue regime, the Wöhler curves did not show clear differences. It was observed decreasing stress amplitude limits as function of life endurance up to the fatigue limit (~$4x10^6$ cycles to failure) and such a value was very similar for both the configurations at a value of the cyclic maximum stress of 200 MPa. Both the L and T welds show a similar behaviour in the crack initiation and growth leading to the conclusion that the FSW process eliminates the effect of rolling direction on the fatigue properties of the welds.

REFERENCES

[1] Mishra, R.S. and Z.Y. Ma. Friction stir welding and processing. Mater. Sci. Engineering, R50 (2005), 1-78.

[2] Bussu, G. and P.E. Irving. The role of residual stress and heat affected zone properties on fatigue crack propagation in friction stir welded 2024-T351 aluminium joints. Int. J. Fatigue, 25 (2003), 77–88.

[3] John, R.and K.V. Jata, K. Sadananda. Residual stress effects on near threshold fatigue crack growth in friction stir welded aerospace alloys. Int. J. Fatigue, 25 (2003), 939-948.

[4] Jata, K.V., K.K. Sankaran and J. Ruschau. Friction-stir welding effects on microstructure and fatigue of aluminum alloy 7050-T7451. Met. Mater. Transactions, 31A (2000), 2181-2192.

[5] Guerra, M., C. Schmidt, J.C. McClure, L.E. Murr and A.C. Nunes. Flow patterns during friction stir welding. Mater. Characterization, 49 (2003), 95– 101.

[6] Ulysse, P. Three-dimensional modeling of the friction stir-welding process. Int. J. Mach. T. Manufacture, 42 (2002), 1549–1557.

[7] Cavaliere, P., A. Squillace, G. Campanile and F. Panella. Effect of welding parameters on mechanical and microstructural properties of AA6056 joints produced by Friction Stir Welding. J. Mater. Proc. Technologies 180 (2006), 263–270.

[8] Rhodes, C.G., M.W. Mahoney nad W.H. Bingel. Effects of Friction Stir Welding on microstructure of 7075 aluminium. Scr. Materialia, 36 (1997), 69–75.

[9] Sato, Y.S., M. Urata, H. Kokawa and K. Ikeda. Hall-/Petch relationship in friction stir welds of equal channel angular-pressed aluminium alloys. Mater. Sci. Engineering, A354 (2003), 298-305.

[10] Berbon, P.B., W. H. Bingel, R.S. Mishra, C.C. Bampton and M.W. Mahoney. Friction Stir Processing: A Tool To homogenize Nanocomposites Aluminum Alloys. Scr. Materialia, 44 (2001), 61–66.

[11] Cavaliere, P., R. Nobile, F. Panella and A. Squillace. Mechanical and microstructural behaviour of 2024-7075 aluminium alloy sheets joined by friction stir welding. Int. J. Mach. T. Manufacture, 46 (2006), 588-594.

[12] Cavaliere, P. and A. Squillace, Effect of welding parameters on mechanical and microstructural properties of dissimilar

AA6082-AA2024 joints produced by Friction Stir Welding. Mater. Sci. Forum 1163-1168 (2006), 519-521.

[13] James, M.N., R. Bradley, H. Lombard and D.G. Hattingh. The relationship between process mechanisms and crack paths in friction stir welded 5083-H321 and 5383-H321 aluminium alloys. Fatig. Fract. Eng. Mater. Structures, 28 (2005), 245-256.

[14] Ericsson, M. and R. Sandstrom. Influence of welding speed on the fatigue of friction stir welds, and comparison with MIG and TIG. Int. J. Fatigue, 25 (2003), 1379-1387.

[15] Dickerson, T.L. and J. Przydatek. Fatigue of friction stir welds in aluminium alloys that contain root flaws. Int. J. Fatigue, 25 (2003), 1399-1409.

[16] Wei, S., C. Hao, J. Chen. Study of friction stir welding of 01420 aluminum–lithium alloy. Mater. Sci. Engineering, A 452–453 (2007), 170–177.

[17] Concise Encyclopedia of Materials Characterization. Ed: R. W. Chan. Elsevier Science Publishers (2005), 707.

[18] Buffa, G., L. Donati, L. Fratini and L. Tomesani. Solid state bonding in extrusion and FSW: Process mechanics and analogies. J. Mater. Proc. Technologie,s 177 (2006), 344-347.

[19] Cavaliere, P., A. Squillace and F. Panella. Effect of welding parameters on mechanical and microstructural properties of AA6082 joints produced by Friction Stir Welding, J. Mater. Proc. Technologies, 200 (2008), 364-372.

[20] Luong M.P.. Thermography: A New Nondestructive Evaluation Method in Fatigue Damage. Mech. Materials, 28 (1998), 155–163.

[21] Hermanson, K.S. and B.I. Sandor. Corrosion Fatigue Modeling Via Differential Infrared Thermography. Ex. Techniques, 22 (1998), 19–21.

[22] Yang, B., P.K. Liaw, H. Wang, J.Y. Huang, R.C. Kuo and J.G. Huang. Thermography: A New Nondestructive Evaluation Method in Fatigue Damage. JOM-e 55 (2003).

[23] Zhang, D. and B.I. Sandor. ASTM STP 1122 (1991), 341–353.

[24] Liaw P.K. Nondestructive Evaluation (NDE) and Materials Properties IV. Warrendale, PA, TMS, (1999).

[25] Tomlison, R.A. and E.J. Olden. Thermoelasticity for the analysis of crack tip stress fields-a review. Strain 35 (1999), 49-55.

[26] Dìaz, F.A., E.A. Patterson, R.A. Tomlison and J.R. Yates. Measuring stress intensity factors during fatigue crack growth using thermoelasticity. Fatig. Fract. Eng. Mater. Structures 27 (2004), 571-583.

[27] Harwood, N. and W.M. Cummings. Thermoelastic Stress Analysis. Adam Hilger 1991.

[28] Shiratori, M., T. Miyoshi, T. Nakanishi, T. Noda and A. Hanada. Detection of Cracks and measurement of Stress intensity factors by infrared video systems. JSME I 33 (1990), 400-408.

[29] Belgen M.H.. Structural Stress Measurements with an Infrared Radiometer. ISA Transactions 6 (1967), 164-177.

[30] P. Cavaliere, G. L. Rossi, R. Di Sante, M. Moretti. Thermoelasticity for the evaluation of fatigue behavior of 7005/Al2O3/10p metal matrix composite sheets joined by FSW. Int. J. Fatigue, 30 (2008), 198–206.

[31] Huang, Y.M., H.H. Abdel Mohsen and R.E. Rowlands. Determination of Individual Stresses Thermoelastically. Ex. Mechanics, 30 (1990), 88-94.

[32] Lesniak J.R.. Thermoelastic data improvements. In: Proceedings of SEM Spring Conference on Experimental Mechanics, Dearborn, Michigan; 1993, 721-729.

[33] Offermann, S., J.L. Beaudoin, C. Bissieux and H. Frick. Thermoelastic Stress Analysis Under Nonadiabatic Conditions. Ex. Mechanics, 37 (1997), 409-413.

[34] John, R., K.V. Jata and K. Sadananda. Residual stress effects on near-threshold fatigue crack growth in friction stir welds in aerospace alloys. Int. J. Fatigue, 25 (2003), 939–948.

[35] H.S. Kong, M.F. Ashby, MRS Bulletin, October 1991, 41.

[36] Di Sante, R., P. Cavaliere, G.L. Rossi and A. Squillace. Thermoelastic analysis of crack propagation in AA6082 Friction Stir Welded Joints. Mater. Sci. Forum 561-565 (2007), 2221-2224.

[37] P. Cavaliere. Crack tip plasticity in plastically graded Ni-W electrodeposited nanocrystalline alloys. Comp. Mater. Science 41 (2008) 440-449.

[38] Cavaliere, P. and F. Panella. Effect of tool position on the fatigue properties of dissimilar 2024-7075 sheets joined by Friction Stir Welding. J. Mater. Proc. Technologies, (2007), doi:10.1016/j.jmatprotec.2007.12.036

[39] Liechty, B.C. and B.W. Webb. Modeling the frictional boundary condition in friction stir welding. J. Mater. Proc. Technologies,doi:10.1016/j.ijmachtools.2008.04.005

[40] Bastier, A., M.H. Maitournam, F. Roger and K. Dang Van. Modelling of the residual state of friction stir welded plates J. Mater. Proc. Technologies, 200 (2008), 25-37.

[41] Zhang, Z. and H.W. Zhang. Numerical studies on controlling of process parameters in friction stir welding. J. Mater. Proc. Technologies, doi:10.1016/j.jmatprotec.2008.01.044

[42] Rajesh, S.R., H.S. Bang, W.S. Chang, H.J. Kim, C.I. Oh and J.S. Chu. Numerical determination of residual stress in friction stir weld using 3D-analytical model of stir zone. J. Mater. Proc. Technologies, 187-188 (2007), 224-226.